

INFORMATION SOCIETIES TECHNOLOGY

(IST)

PROGRAMME



Project Number

10954

Project Title:

Virtual Animation of the Kinematics of the Human for Industrial, Educational and Research Purposes

Title of deliverable

D3.2. Technical Report on Data Collection Procedure



PART I

Project Number: 10954

Project Title : Virtual Animation of the Kinematics of the Human for Industrial, Educational and Research Purposes

Deliverable Type: RP

Deliverable Number: D3.2

Contractual date of delivery to the Commission: M10

Actual date of delivery to the Commission: M11

Title of deliverable: Technical Report on Data Collection Procedure

Work package contributing to the deliverable: WP3

Nature of the deliverable: REPORT

Authors:

<p><u>Deliverable Leaders:</u></p> <ul style="list-style-type: none"> • <i>Marco VICECONTI, Fulvia TADDEI</i> Istituti Ortopedici Rizzoli Via di Barbiano 1/10 40136 Bologna - I <p><u>Participants:</u></p> <ul style="list-style-type: none"> • <i>Serge VAN SINT JAN, Victor CHOLUKHA, Isam HILAL, Patrick SALVIA</i> University of Brussels (CP 619) Lennik Street, 808 1070 Brussels - BE • <i>Feng DONG, Gordon CLAPWORTHY</i> De Montfort University Hammerwood Gate, Kents Hill MK7 6HP Milton Keynes – UK 	<ul style="list-style-type: none"> • <i>Alberto LEARDINI, Stefano BRECCIA, Lorenzo CHIARI</i> Istituti Ortopedici Rizzoli Via di Barbiano 1/10 40136 Bologna – I • <i>Aurelio CAPPOZZO, Ugo DELLA CROCE</i> Università degli Studi di Sassari V.le S. Pietro 43/b 07100 Sassari – I
---	---

Abstract:

The present document summarises the procedures that will be used in the VAKHUM project to collect and process anatomical and functional data. The whole process is organised in a simple, well-defined data flow that specifies the sequence of data collection and processing operations as well as the logical connections between separate collection/processing phases. Each method is briefly described, qualified in terms of accuracy and/or repeatability and its interfaces in the data flow are formalised with all necessary specifications. The majority of the methods in use were already established at the site of one of the Partner. The maturity of these methods is evident in their qualification, which is extensive and accurate. Sample sets have been collected and used to test the whole workflow. No problems have emerged so far. The preparation of this deliverable has demonstrated how the European dimension of the project can ensure the critical mass of experience and knowledge required to address problems of this complexity.

Keyword list:

Joint morphology, joint kinematics, 3D reconstruction, gait analysis, stereophotogrammetry, finite elements, automatic mesh generation.

INDEX

INDEX.....	1
SUMMARY	1
1 INTRODUCTION.....	2
2 DATA COLLECTION AND PROCESSING.....	3
2.1 CT data collection	4
2.1.1 Description of the procedure.....	4
2.1.2 Methodological qualification.....	5
2.1.3 Data processing flow interfaces.....	6
2.2 Data alignment	8
2.2.1 Description of the procedure.....	8
2.2.2 Methodological qualification.....	9
2.2.3 Data processing flow interfaces.....	10
2.3 CT data segmentation.....	12
2.3.1 Description of the procedure.....	12
2.3.2 Methodological qualification.....	14
2.3.3 Data processing flow interfaces.....	14
2.4 3D Reconstruction (bone models).....	16
2.4.1 Description of the procedure.....	16
2.4.2 Methodological qualification.....	16
2.4.3 Data processing flow interface.....	17
2.5 Collection of Limb kinematics data.....	19
2.5.1 Description of the procedure.....	20
2.5.2 Methodological qualification.....	21
2.5.3 Data processing flow interfaces.....	22
2.6 Collection of Joint kinematics data	24
2.6.1 Description of the procedure.....	24
2.6.2 Methodological qualification.....	25
2.6.3 Data processing flow interfaces.....	25
2.7 Intra CT registration for collection of joint kinematics data.....	27
2.7.1 Description of the procedure.....	27
2.7.2 Methodological qualification.....	28
2.7.3 Data processing flow interfaces.....	29
2.8 Muscle modelling.....	30
2.8.1 Description of the procedure.....	30
2.8.2 Methodological qualification.....	33
2.8.3 Data processing flow interfaces.....	35
2.9 Finite element mesh generation	37
2.9.1 Description of the procedure.....	37
2.9.2 Methodological qualification.....	38
2.9.3 Data processing flow interfaces.....	39
3 REFERENCES.....	41

SUMMARY

The present document summarises the procedures that will be used in the VAKHUM project to collect and process anatomical and functional data. The whole process is organised in a simple, well-defined data flow that specifies the sequence of data collection and processing operations as well as the logical connections between separate collection/processing phases.

Each method is briefly described and qualified in terms of accuracy and/or repeatability. Particular attention is given to the connection with the subsequent processing phases. This connection is defined not only from a logical point of view; specifications are also given on how to organise the data flow between the separate phases, which frequently involve the other Consortium members.

The majority of the methods in use were already established at a site of one of the Partner. The maturity of these methods is evident in their qualification, which is extensive and accurate. Only the protocol for muscle segmentation and 3D modelling has been developed during the project. Although the methods proposed fulfil the project requirements, alternative approaches are currently under investigation to verify if they can reduce the human effort currently required. Thus, it is still possible that the method described here may be modified later in the project. In theory, other minor modifications may also be imposed by the procedures for registration to be developed in WP4. However, at the present stage this seems unlikely.

Sample sets have been collected and then used to test the whole workflow. No problems have emerged so far. A temporary data repository has been established at the ULB VAKHUM web site, where the resulting models will be archived until the database infrastructure is available. All partners will be able to access these models for testing and demonstration.

The preparation of this deliverable has demonstrated how the European dimension of the project can ensure the critical mass of experience and knowledge required to address problems of this complexity. Each problem we faced in defining the data collection procedure was openly discussed on the VAKHUM mailing-list and a solution was always found in a program, a method, a technique already available to one partner or to another. The synergy of the collaboration was evident.

1 INTRODUCTION

The present deliverable is aimed at describing the data-collection procedure to be used during the VAKHUM Project.

The individual data-collection techniques were described in great detail and discussed in the light of the international state of the art in Deliverable D3.1. Such procedures, already implemented at the Partners' sites, were thoroughly revised to take account of the project workflow. All data-collection and data-processing steps were identified, and the relative protocols were revised for such integration.

It can be immediately stated that such integration of the various methods at the user site was relatively smooth and required only minimal adjustments to achieve a good integration. This confirms the quality of the procedures each partner already used at its site. Only the various aspects of muscle modelling (data collection, segmentation, mathematical smoothing) are new and need further improvements.

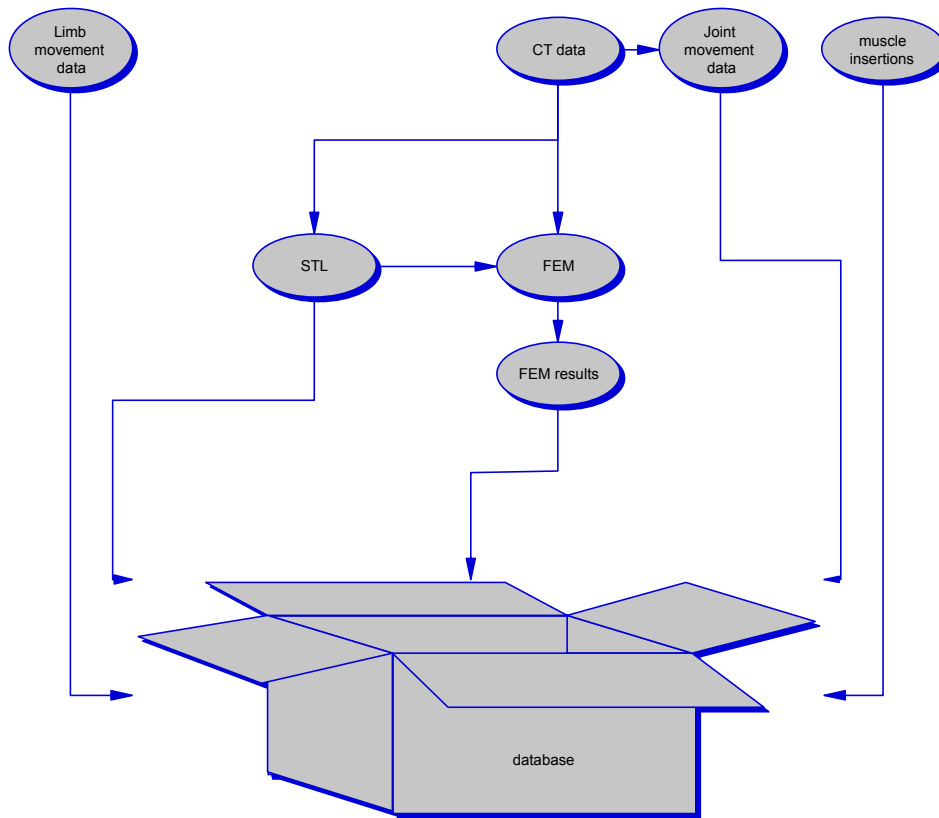
The present report will be structured to follow the data workflow. Each data acquisition/elaboration step will be briefly described in a separate section (as detailed descriptions are given in D3.1) and then fully qualified in term of accuracy and/or repeatability. The section will be completed by a definition of the interfaces with each other data acquisition/elaboration step, defined in terms of common data representation and exchange formats.

The anatomy data collection is initiated by CT data collection, followed by data alignment and CT data segmentation, intra CT registration for joint kinematics data collection, eventual digital bone landmarking for limb kinematics data collection and finite element mesh generation. CT data, 3D surfaces, landmarks co-ordinates and finite element meshes are stored in the VAKHUM Data Repository. The joint kinematics data collection and the limb kinematics data collection establish two separate threads, in which data are directly stored in the VAKHUM Data Repository.

This data collection/elaboration flow does not account for inter-subject registration. This aspect will be specifically addressed by WP4. At the end of that workpackage the data-collection procedure may be revised in line with any new techniques developed during the research. However, it is expected that the basic data-collection procedures, as well most of the data flow interfaces, described here will remain unchanged.

2 DATA COLLECTION AND PROCESSING

The data flow can be effectively represented with the following scheme.



In the following paragraphs each step of data acquisition and processing, when appropriate, will be discussed in greater details. The first aspect addressed is the CT data collection, since the data are used in many different processing steps.

2.1 CT DATA COLLECTION

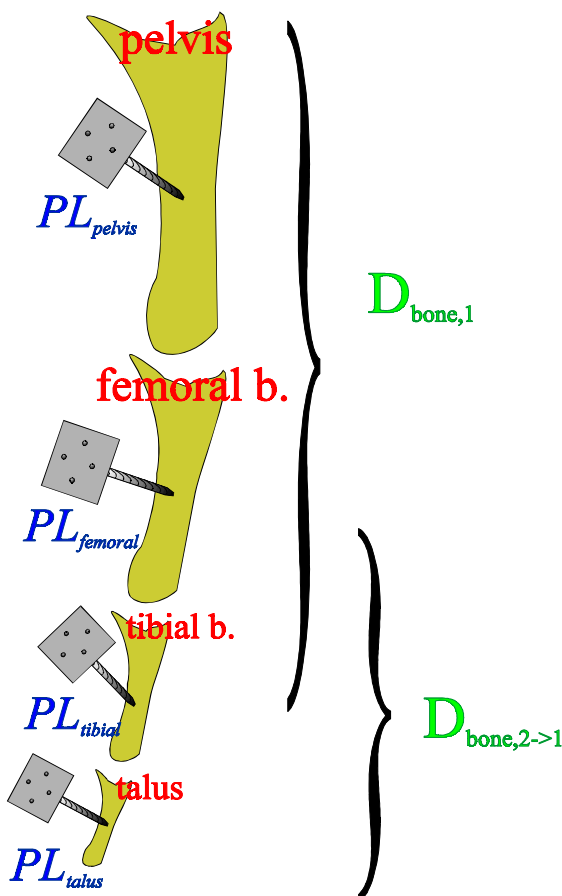
The computerized tomography (or CT) data collection provides most of the morphological data used within the project. The CT installation used for VAKHUM is an *Elscint Spiral Twin Flash*[®]. It allows simultaneous dual-slice scanning thanks to a dual slice beam. The maximal scanning length is 1000 mm; the lowest slice thickness is 0.5 mm; the scan diameter is from 180 to 500 mm.

2.1.1 Description of the procedure

Most datasets are collected from *in vitro* experiments; it is anticipated that some *in vivo* experiments will be performed as well. Most imaging parameters are similar for both experiments.

2.1.1.1 IN VITRO EXPERIMENT

Fresh frozen cadavers are used. Sawing occurred above the pelvis and both limbs are kept. Thawing occurred 48 hours before medical imaging. Soft tissues remain untouched.



Reference plates (see Figure 1 beside and Figure 3 in Viceconti, 2000) are inserted into the following bone segments: PL_{pelvis} in the pelvis, $PL_{femoral}$ in the femoral bone, PL_{tibial} in the tibial bone and PL_{talus} in the talus. This will allow alignment of the structures if several datasets of the same specimen are necessary (see below).

The specimen is then set on a large wooden board without any special attachments. All joints are aligned along the conventional anatomical neutral position (note: because of the surrounding soft tissue this cannot be fully guaranteed).

Figure 1. Experimental setup for acquisition of the morphological data (CT imaging). See text for explanations.

Scanning parameters are as follows:

Pitch	1.5 D
Slice Thickness	Epiphysis (joint level): 2.7 mm Diaphysis: 5.0 mm
Slice Increment	Epiphysis (joint level): between 0.7 mm and 1.0 mm Diaphysis: between 3.0 mm and 4.0 mm
Image matrix	512 ² or 768 ²
Scan diameter	250 mm or 430 mm

If the specimen length is greater than 1000 mm (which is the maximal scanning length allowed by the system, see above) then data collection must be performed in two steps ($D_{bone,1}$, $D_{bone,2}$) and an alignment of both datasets must be performed later (see 2.2 *Data alignment*) using the reference plates Pl inserted into the bones. Step 1 ($D_{bone,1}$) includes the area from above the iliac crests to the upper part of the tibial bone diaphysis, while step 2 ($D_{bone,2}$) includes the area from the distal part of the femoral diaphysis to the whole foot. Both steps show the reference plate Pl_{tibial} inserted within the tibial bone; the latter allows the alignment of both steps (see 2.2 *Data alignment*).

2.1.1.2 IN VIVO EXPERIMENT

With volunteers, the same parameters as above are used. If necessary, a reference plate will be attached to the subject’s limb by strapping. For ethical reasons, no CT imaging of the pelvis can be performed on healthy volunteers. An alternative could be found if volunteers, who have to undergo a CT of the pelvis for medical reasons, are requested to permit image acquisition to be extended to the full limb. As of 20 November 2000, the local ethical committee still has to approve this.

2.1.2 Methodological qualification

- High-contrast spatial resolution:

Mode	Scan technique	Resolution MTF: modulation transfer function lp/cm: line pairs /cm
Ultra-high mode	120 kVp, 200 mA, 1 sec, 2.5 mm slice width, 512 ² matrix, 250 mm FOV, zoom 2, detail (E) filter	9.4 lp/cm @ 50% MTF 16.7 lp/cm @ 10% MTF 20.0 lp/cm @ cut-off
High mode	120 kVp, 200 mA, 1 sec, 2.5 mm slice width, 512 ² matrix, 430 mm FOV, zoom 2.5, detail (E) filter	7.4 lp/cm @ 50% MTF 12.0 lp/cm @ 10% MTF 14.0 lp/cm @ cut-off
Standard mode	120 kVp, 300 mA, 1 sec, 10 mm slice width, 512 ² matrix, 430 mm FOV, zoom 1.8, detail (D) filter	5.4 lp/cm @ 50% MTF 8.5 lp/cm @ 10% MTF 11.0 lp/cm @ cut-off

- Noise: 0.29 % as measured on the system phantom in standard mode (standard (EB) filter, see above table for other parameters).
- Low contrast detectability: 0.25 % for a 3.0 mm pin as measured on the system phantom in standard mode (standard (EB) filter, see above table for other parameters).
- Absorption measurement range: -1000 to +3095 Hounsfield units.

2.1.3 Data processing flow interfaces

The CT data are used for:

- Creation of 3D models by segmentation;
- joint landmark calibration;
- finite element analyses;
- database storage.

The first dataset ($D_{bone,1}$) is used to obtain morphological data of the pelvis, femoral bone and patella. The second dataset ($D_{bone,2}$) is used to obtain data of the tibial bone, fibula and all foot components. Note both datasets need to be in alignment in order to obtain a full lower-limb skeleton (see 2.2 *Data alignment*).

Data description

The CT data should be written in terms of Hounsfield Units, so as to be independent of the particular CT scanner, if possible. If not, then the *Rescale Intercept* and *Rescale Slope* fields in the DICOM header must be saved. If density calibration is provided it is important to have a text file in which the densities of the different regions of the adopted phantom are given.

Data format

The CT datasets will be passed to other processing units via the DICOM3 format.

A typical DICOM3 file header shows at least the following tags (tag number is between round brackets). A more detailed description can be found at <http://www2.ios.com/~dclunie/dicom-status/status.html>, Part 6: data dictionary:

Identifying Group Length (0008,0000)	1	UL [418]
Image Type (0008,0008)	1-n	CS [ORIGINAL\PRIMARY\AXIAL\CT]
SOP Class UID (0008,0016)	1	UI [1.2.840.10008.5.1.4.1.1.2]
SOP Instance UID (0008,0018)	1	UI [1.2.840.113704.6.85572991186561.20000421.58729.10002900032]
Study Date (0008,0020)	1	DA [2000.04.21]

Image Date	(0008,0023)	1	DA	[2000.04.21]
Study Time	(0008,0030)	1	TM	[17:25:32]
Image Time	(0008,0033)	1	TM	[17:25:32]
Accession Number	(0008,0050)	1	SH	[85572991186561]
Modality	(0008,0060)	1	CS	[CT]
Manufacturer	(0008,0070)	1	LO	[ELSCINT]
Institution Name	(0008,0080)	1	LO	[INSTITUT J. BORDET]
Referring Physician's Name	(0008,0090)	1	PN	[VANSINTJAN]
Manufacturer's Model Name	(0008,1090)	1	LO	[CT TWIN]
Patient Group Length	(0010,0000)	1	UL	[46]
Patient's Name	(0010,0010)	1	PN	[LEG1]
Patient's ID	(0010,0020)	1	LO	[1]
Patient's Birth Date	(0010,0030)	1	DA	[2000.04.21]
Acquisition Group Length	(0018,0000)	1	UL	[156]
Slice Thickness	(0018,0050)	1	DS	[2.7]
KVP	(0018,0060)	1	DS	[120]
Spacing Between Slices	(0018,0088)	1	DS	[1.0]
Data Collection Diameter	(0018,0090)	1	DS	[250]
Reconstruction Diameter	(0018,1100)	1	DS	[250.00]
Distance Source To Detector	(0018,1110)	1	DS	[1093]
Distance Source To Patient	(0018,1111)	1	DS	[630]
Gantry/Detector Tilt	(0018,1120)	1	DS	[0.0]
Scan Arc	(0018,1143)	1	DS	[403]
X-ray Tube Current	(0018,1151)	1	IS	[200]
Exposure	(0018,1152)	1	IS	[135]
Filter Type	(0018,1160)	1	SH	[F]
Patient Position	(0018,5100)	1	CS	[HFS]
Image Group Length	(0020,0000)	1	UL	[356]
Study Instance UID	(0020,000D)	1	UI	[1.2.840.113704.6.85572991186561.20000421]
Series Instance UID	(0020,000E)	1	UI	[1.2.840.113704.6.85572991186561.20000421.58729]
Study ID	(0020,0010)	1	SH	[85572991186561]
Series Number	(0020,0011)	1	IS	[58729]
Acquisition Number	(0020,0012)	1	IS	[1]
Image Number	(0020,0013)	1	IS	[29]
Patient Orientation	(0020,0020)	2	CS	[L\^P]
Image Position (Patient)	(0020,0032)	3	DS	[-125.00\^-103.30\^396.40]
Image Orientation (Patient)	(0020,0037)	6	DS	[1.00000000\^0.00000000\^-0.00000000\^-0.00000000\^1.00000000\^0.00000000]
Frame of Reference UID	(0020,0052)	1	UI	[1.2.840.113704.6.85572991186561.58725.10000100512]
Slice Location	(0020,1041)	1	DS	[396.4]
Image Presenta... Group Length	(0028,0000)	1	UL	[192]
Samples per Pixel	(0028,0002)	1	US	[1]
Photometric Interpretation	(0028,0004)	1	CS	[MONOCHROME2]
Rows	(0028,0010)	1	US	[512]
Columns	(0028,0011)	1	US	[512]
Pixel Spacing	(0028,0030)	2	DS	[0.488\^0.488]
Zoom Factor	(0028,0031)	2	DS	[1.00\^1.00]
Zoom Center	(0028,0032)	2	DS	[0.00\^0.00]
Bits Allocated	(0028,0100)	1	US	[16]
Bits Stored	(0028,0101)	1	US	[12]
High Bit	(0028,0102)	1	US	[11]
Pixel Representation	(0028,0103)	1	US	[0]
Window Center	(0028,1050)	1-n	DS	[56]
Window Width	(0028,1051)	1-n	DS	[426]
Rescale Intercept	(0028,1052)	1	DS	[-1000]
Rescale Slope	(0028,1053)	1	DS	[1]
Pixel Data Group Length	(7FE0,0000)	1	UL	[524296]
Pixel Data	(7FE0,0010)	1	OW	[262144 * 2 bytes at offset 2786 (0xae2) in jambe_ok.dcm using bflags 0x2501 (has little endian str_size_2 implicit_hint)]

In the VAKHUM Data Repository multiple instances of the CT dataset may be made available for internal use. Rectilinear grid and raw file format will be the most used (Schroeder, 1998).

2.2 DATA ALIGNMENT

Because of the limited scanning length of the CT installation, it is usually necessary to collect several datasets ($D_{bone,1}$, $D_{bone,2}$) for a full lower limb (see 2.1 CT data collection). By the nature of the data collection, these datasets are not aligned. The following section explains how to solve this problem.

2.2.1 Description of the procedure

As mentioned above, the $D_{bone,1}$ and $D_{bone,2}$ datasets both show the tibial reference plate Pl_{tibial} , which includes four aluminium markers m_j $\{j: 0 \rightarrow 3\}$ (diameter: 3mm).

Marker location: The following procedure is applied on both $D_{bone,1}$ and $D_{bone,2}$ independently. In order to process the datasets automatically, an object-recognition method is utilized. The method proceeds as follows. First, a Sobel edge-gradient filter (Russ, 1995) is applied on the dataset $D_{bone,i}$ $\{i: 1 \rightarrow 2\}$ to enhance the limits of the objects of interest in the dataset slices. The markers appear as circles in the filtered dataset $D_{bone,i}^{filter}$ which is then analysed by a modified object-recognition algorithm based on hypothesis constraints including marker intensity, marker diameter and circularity (Yip, 1992; Lam, 1996). When the centroid of a circle is located in $D_{bone,i}^{filter}$, its spatial coordinates are used as a seed into the original $D_{bone,i}$ to start a region growing, which determines the 3D coordinates of the spherical marker centroid with sub-pixel accuracy (Ellis, 1996). Eventually, the spatial coordinates of the 4 m_j markers are found within both $D_{bone,1}$ and $D_{bone,2}$ datasets ($m_{j,1}$ and $m_{j,2}$)

Alignment matrix: Using the coordinates of both $m_{j,1}$ and $m_{j,2}$, an alignment matrix $C = \begin{bmatrix} R_c & Tr_c \\ 0 & 1 \end{bmatrix}$ between $D_{bone,1}$ and $D_{bone,2}$ is found. C is determined by using the above four $m_{j,1}$ and $m_{j,2}$ points in a Singular Value Decomposition procedure (Söderkvist, 1993; Press et al., 1992). Thus, the relationship between $D_{bone,1}$ and $D_{bone,2}$ is now fully defined. Alignment of $D_{bone,2}$ with $D_{bone,1}$ occurs according: $D_{bone,2 \rightarrow 1} = C D_{bone,2}$.

2.2.2 Methodological qualification

Marker location: A CT installation phantom is used to quantify the accuracy of the marker location method. A phantom is classically used to calibrate and quantify CT accuracy. It contains several cylindrical areas, of known dimensions, made of different materials (Figure 2).

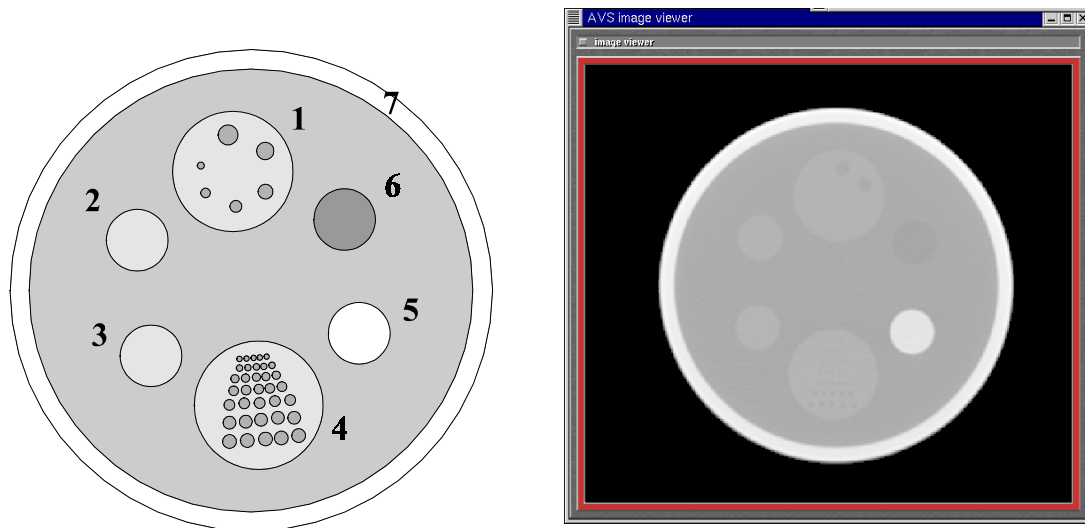


Figure 2. CT Phantom. Left: composition; right: actual CT image of the phantom using the parameters-mentioned below (see Section 2.1) with scan diameter= 430 mm and scan matrix = 512^2 .

Pin 1: Nylon (Aculon) body with six smaller Lexan pins of 3, 4, 5, 6, 7 and 8 mm diameter respectively.

Pin 2: Polyethylene pin (\varnothing : 25 mm).

Pin 3: Teflon pin (\varnothing : 25 mm).

Pin 4: Perspex pin with seven rows of holes of different diameters (row 1: 1.00 mm, row 2: 1.25 mm, row 3: 1.50 mm, row 4: 1.75 mm, row 5: 2.00 mm, row 6: 2.50 mm, row 7: 3.00 mm). Each row has five equidistant holes of the same diameter (distance between holes = row 1: 2.0 mm, row 2: 2.50 mm, row 3: 3.00 mm, row 4: 3.50 mm, row 5: 4.00 mm, row 6: 5.00 mm, row 7: 6.00 mm).

Pin 5: Lexan pin (\varnothing : 25 mm).

Pin 6: Perspex pin (\varnothing : 25 mm).

Pin 7: PVC.

The above procedure for marker location has been applied to the rows of holes included in the Perspex pin of the phantom (Figure 2, # 4). Distances between each estimated centroid in a row and all the other hole centroids of the same row have been processed, averaged and compared to the distance given by the constructor (see Figure 2). Results show (Figure 3) that sub-voxel accuracy is achieved from a diameter of 1.5 mm (row 3).

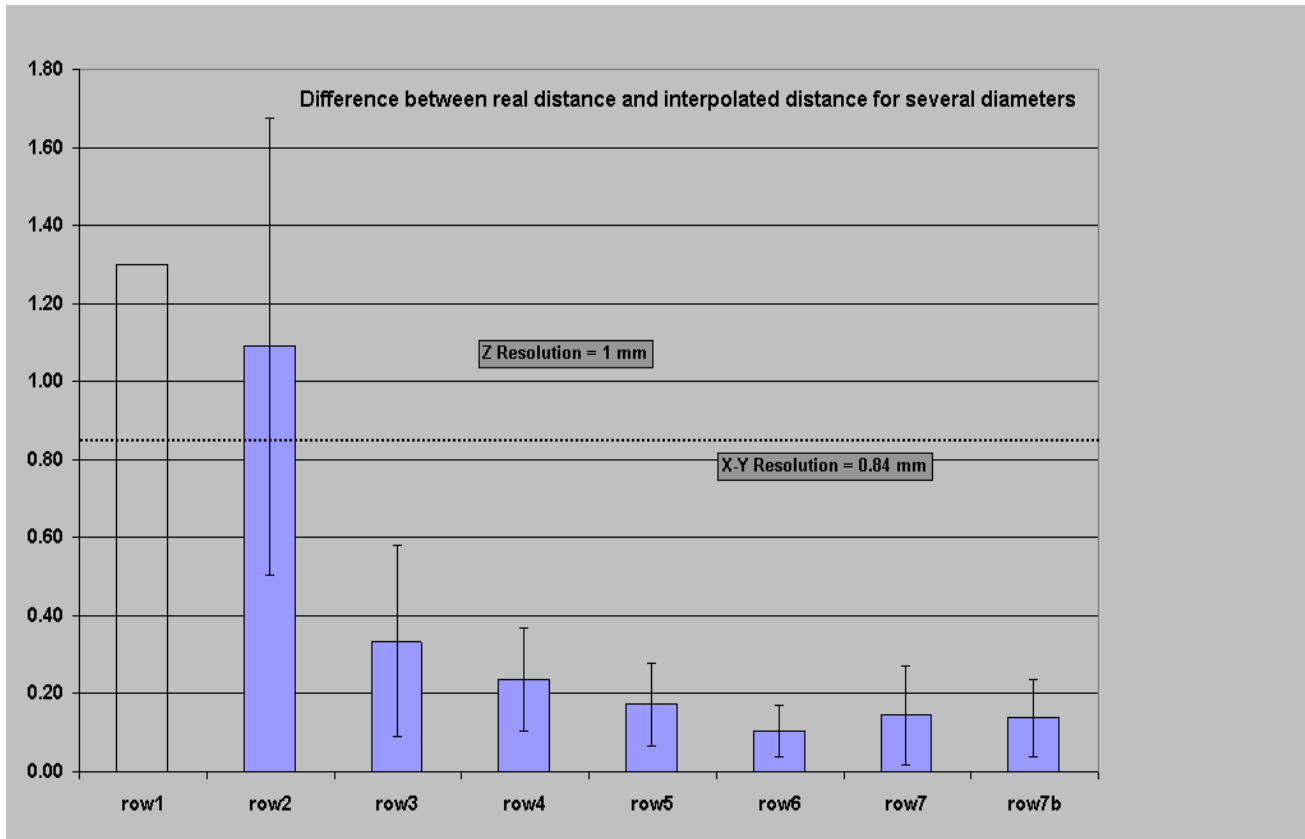


Figure 3. Accuracy of the centroid location method. The averaged difference (in mm) between the real distance of the centre of holes (Figure 2) and the estimated distance is shown for each row. The dataset resolution, i.e. voxel size, is also indicated. For the smallest holes (row1) the protocol for centroid estimation failed. For the other structures, apart from the holes in row 2, the averaged difference is less than the dataset resolution. Row 7 has been processed twice (row7 and row7b) for repeatability. Note that the aluminium markers used for VAKHUM have a diameter similar to rows 5, 6 and 7.

Alignment matrix: The RMS error in the determination of C is satisfactory. Preliminary results show an average RMS error of 0.76 mm.

2.2.3 Data processing flow interfaces

As mentioned above, $D_{bone,2}$ is not in alignment with $D_{bone,1}$. Alignment of $D_{bone,2}$ along $D_{bone,1}$ is performed using the alignment matrix C. This alignment can be processed at several levels (e.g., on the original image dataset or on the vertices of the 3D models). Within VAKHUM, some 3D models are obtained from the original $D_{bone,2}$ dataset, which is not in alignment with $D_{bone,1}$. Only then, the vertices of these particular 3D models are transformed using the above C matrix.

Data description

Both the C matrix and the centroid of the markers (in both $D_{bone,1}$ and $D_{bone,2}$) of the tibial reference plate Pl_{tibial} will be available from the same directory as the original image datasets $D_{bone,1}$ and $D_{bone,2}$.

Data format

The ASCII data file will show:

1. firstly, the C matrix: $C_{2 \rightarrow 1} = \begin{bmatrix} R_c & Tr_c \\ 0 & 1 \end{bmatrix}$,
2. then, the centroid of the four markers of the tibial reference plate Pl_{tibial} in $D_{bone,1}$,
3. finally, the centroid of the four markers of the tibial reference plate Pl_{tibial} in $D_{bone,2}$.

2.3 CT DATA SEGMENTATION

The first step to be performed on the CT dataset is the identification, and segmentation, of the region of interest. The 3D surface model of the bone segment under investigation should be extracted from the dataset. Several methods of segmentation are available: automatic, semi-automatic and fully manual. Within VAKHUM, these methods are applied according to the structure of interest and will depend upon the contrast of the boundaries between adjacent structures. Automatic segmentation is used for the knee joint and where bones are not adjacent to other structures of similar intensity. Semi-automatic procedures will be applied to the hip and ankle joints. A manual procedure will be applied to other structures (e.g. muscles, see 3.8 *Muscles Modelling*) and when bone segmentation is complicated by the presence of artefacts. All segmentation procedures are performed within the original medical-imaging reference frame.

2.3.1 Description of the procedure

2.3.1.1 AUTOMATIC PROTOCOL

This procedure performs the segmentation of bone structure automatically with little need for human intervention. It is fast (typically less than 15 minutes for a full knee dataset), but unfortunately can only be applied when adjacent structures show clearly-separated boundaries.

- 1) the full image (see 2.1 *CT Data Collection*) dataset to be segmented is opened in the current session; the dataset is stored in memory in an rectilinear data structure (Schroeder, 1997) including both the original intensity and the original spatial coordinates of the voxels,
- 2) a view where all structures to be segmented are visible on the screen is selected (typically either a frontal view or a sagittal view),
- 3) using the mouse cursor, the structure of interest is selected by a single click in the current view,
- 4) from the cursor position the system will read, in the above rectilinear data structure, the selected voxel intensity I_v ; the user then sets a lower-intensity threshold I_{low} and a higher intensity threshold I_{high} , with $I_{low} > I_v > I_{high}$,
- 5) from the selected voxel, or *seed*, the protocol will analyse the intensity I_k of each voxel within the kernel, or neighbourhood, around the seed; if a voxel in the kernel has an

intensity I_k within the user thresholds ($I_{low} > I_k > I_{high}$) then this voxel is included in the current structure,

- 6) step 5 is automatically repeated (“*the seed is growing*”) from the last selected voxel until no adjacent voxel in the neighbourhood has an intensity within the above threshold limits.

When successful, only the structure of interest is segmented; if the protocol fails a semi-automatic method is used (see below).

2.3.1.2 SEMI-AUTOMATIC PROTOCOL

Initially, the automatic protocol (see above) is performed on the dataset. If the operation is successful, the semi-automatic protocol is not necessary, otherwise the following is applied. In general failure of the automatic protocol occurs because the selected values for the threshold parameters do not allow different structures to be identified, which most frequently occurs when borders are very close of each other and of similar intensity. In such a case, the following steps are applied.

- 7) New intensity parameters (I_{low} , I_v , I_{high}) and/or seed location are selected (see step 3, 4, 5 and 6 above) interactively. If the segmentation still does not give satisfactory results after several attempts, then the steps 8 and 9 are applied.
- 8) The intensity range between I_{low} and I_{high} is reduced. This generally leads to isolation of the selected structure. On the other hand, because of the reduced intensity range, voxels of interest are often not selected, and the 3D models obtained after the segmentation will show holes.
- 9) The holes are then manually filled using the original intensity of the voxels, which were discarded at the previous step.

2.3.1.3 MANUAL PROTOCOL

In some cases, structures can be segmented only by manual segmentation (e.g. muscular structures).

The protocol is as follows:

- 1) the full image (see *2.1 CT Data Collection*) dataset to be segmented is opened in the current session; the dataset is stored in memory in an rectilinear data structure (Schroeder, 1997) including both the original intensity and the original spatial coordinates of the voxels,
- 2) a first slice where the structure of interest is visible on the screen is selected,
- 3) using the mouse cursor, the user clicks sequentially along the structure contour,
- 4) the system will read, from the above rectilinear data structure, the spatial coordinates of the selected voxels,
- 5) when the contour of the structure in the current slice is fully digitised, the user selects the next slice and repeat step 4- until the whole structure is processed.

2.3.2 Methodological qualification

See section *2.4, 3D Reconstruction*, for the qualification of the automatic and semi-automatic protocols. See section *2.8, Muscle Modelling*, for the manual protocol.

2.3.3 Data processing flow interfaces

The segmented image datasets will be used for:

- 3D reconstruction of bone models;
- 3D reconstruction of muscle models.

Data description

In both the automatic and the semi-automatic segmentation protocols, the output forms a rectilinear data structure (Schroeder, 1997) including both the original intensity and the original spatial coordinates of the voxels. Only voxels of the segmented structure are present in the dataset.

Output from the manual segmentation protocol contains the external surface of the segmented structures.

Data format

Raw segmented data will not be exchanged. Data-model exchange will occur after reconstruction (see Section 2.4, *3D Reconstruction (bone models)*, and Section 2.8, *Muscle Modelling*).

2.4 3D RECONSTRUCTION (BONE MODELS)

2.4.1 Description of the procedure

For each particular segmented rectilinear dataset, an algorithm based on the Marching Cubes (Lorensen, 1987) is used to obtain the isosurface 3D models.

Note: in the output of both the automatic and the semi-automatic segmentation protocols, all voxels within the selected structures should be available to facilitate the selection of the external envelope during the 3D reconstruction process. If some voxels are missed within the structures, then not only will the envelope be reconstructed, but also some additional features within the bone. This will increase the size of the 3D object and, hence, its processing (e.g. motion simulation) will be slower than with the envelope only.

2.4.2 Methodological qualification

The following procedure has been applied to quantify the accuracy of the automatic and semi-automatic segmentation protocols. From the CT dataset of the phantom used previously (chapter 2.2 *Data alignment*), all cylindrical areas were segmented and 3D models were obtained using the method mentioned in the current chapter (Figure 4). These cylinders have well-known diameter and height. Therefore, their exact surface area can be found from $surface = 2\pi \cdot radius \cdot height$ and compared to the total surface of the 3D models obtained by the addition of their facets.

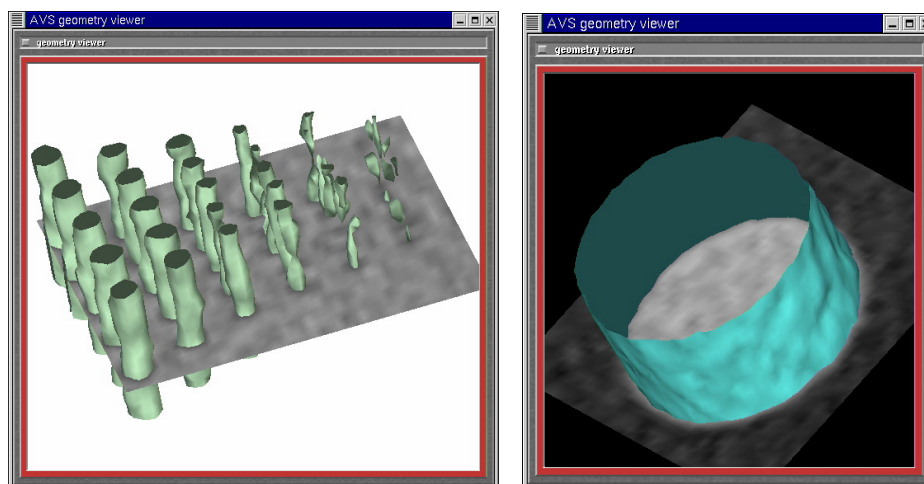


Figure 4. Phantom surface. Left: the seven rows of holes in pin 4. Right: pin 3.

Maximal and minimal deviations were 114.8 mm² and 0.08 mm² respectively, which is a maximal and minimal error of 4.87% and 0.01% respectively (Table 1). The error is dependant of the quality of the boundaries, i.e. the contrast, between the structure of interest and the remaining of the dataset. The nature of the structure of interest is also of importance. Though it is difficult to quantify the real surface of a bone, we can anticipate that error on the final bone models will be in the same range as these results because 1- contrast between bone structure and surrounding soft tissue is normally high and 2- bone boundaries are normally well defined in a CT image dataset.

	<u>pin 6</u>	<u>pin 5</u>	<u>pin 3</u>	<u>pin 2</u>	<u>pin 1</u>	<u>Lexan 7mm</u>	<u>Lexan 8mm</u>	<u>row 7</u>	<u>row 6</u>	<u>row 5</u>	<u>row 4</u>	<u>row 3</u>	<u>max</u>	<u>min</u>
<u>Contrast</u>	-108	572	94	75	52	-47	-71	-71	-71	-61	-54	-43	/	/
<u>Height</u>	15.00	15.00	15.00	15.00	15.00	15.00	15.00	15.00	15.00	15.00	15.00	11.50	/	/
<u>Diameter (mm)</u>	25.00	25.00	25.00	25.00	50.00	7.00	8.00	3.00	2.50	2.00	1.75	1.50	/	/
<u>Surface (mm²)</u>	1178.10	1178.10	1178.10	1178.10	2356.19	329.87	376.99	141.37	117.81	94.25	82.47	49.87	/	/
<u>Interpolated (mm²)</u>	1221.99	1178.24	1184.48	1178.02	2471.00	328.35	376.11	141.21	117.53	94.42	82.95	49.70	/	/
<u>Difference</u>	43.89	0.14	6.38	0.08	114.80	1.52	0.88	0.39	0.28	0.19	0.48	0.26	<u>114.80</u>	<u>0.08</u>
<u>% error</u>	3.73	0.01	0.54	0.01	4.87	0.46	0.23	0.28	0.24	0.20	0.59	0.48	<u>4.87</u>	<u>0.01</u>

Table 1. Difference between real and interpolated surface. The surfaces of the pins illustrated in Figure 2 are shown in the row “Interpolated”, while real surface is in row “Surface” (the latter is processed from both “Height” and “Diameter”. “Contrast” is the difference between the average intensity of the object of interest and the average intensity of its neighbourhood. The columns “row i” are the average surface for each row in pin 4; because of their limited diameter, row 1 and 2 showed unsatisfactory 3D reconstruction, see Figure 3, and were not processed further

2.4.3 Data processing flow interface

The 3D external surface of the bone segment will be stored in the database and will be used for:

- Finite element mesh generation;
- Skeletal Landmark registration.

By Skeletal Landmarks (SLs), we indicate the landmarks used by ULB for the registration of the joint geometry and the CT dataset; this in order to distinguish them from the Anatomical Landmarks (ALs) referred to in the Gait Analysis protocol.

Data description

The external surface of each bone segment should be represented by a tiled surface. The surface need not be “watertight”, and little gaps or overlaps or even slightly non-conforming triangles are allowed.

Data format

The tiled surface will be saved in a STL (Stereolithography) ASCII file format. This format is becoming an international standard since it is used in Rapid Prototyping applications, and many commercial softwares are now able to read it. The STL format can be an ASCII or binary file. It is a list of the triangular surfaces that describe a computer-generated solid model.

2.5 COLLECTION OF LIMB KINEMATICS DATA

The orientation and position of a bone in space, dealt with as if it was a rigid body, entails the definition of an orthogonal frame, named the *bone-embedded frame*, which is rigid with the bone and numerically described with respect to a given observer using a position vector and an orientation matrix or an orientation vector.

For practical purposes, bone-embedded frames should meet the following requirements:

- 1) Their determination from experimental data should be repeatable both inter- and intra-individually.
- 2) In view of the quantitative description of the relevant joint kinematics, they should possibly incorporate, or permit the determination of, suitable axes with respect to which both rotations and translations of the joint may be defined (*joint axes*).
- 3) Since the analysis of the limb will be dynamic, they should permit an easy implementation of the estimation techniques aimed at the location of the body-segment centre of mass and principal axes of inertia. In addition, sufficient information must be available to locate the reference system with respect to which the intersegmental loads are calculated.
- 4) Requirements associated with the description of the muscle and ligament line of action and the location and orientation of the articulation surfaces must also be taken into careful consideration.

It is evident that frames rigidly associated with the anatomy of the bone meet the above-mentioned requirements. Their identification will therefore be based on the location of a number of anatomical landmarks (ALs). A bone-embedded frame that meets these requirements is termed an anatomical frame (BAF).

All stereophotogrammetric techniques entail indicating target points by convenient markers, the physical realization of which depends upon the particular technique used. Here we assume the these markers are associated with cutaneous (external) ALs. The marker points have to be selected according to experimental requirements that often do not match the ones reported above for ALs.

The frame determined using marker-point coordinates is referred to as the **bone-embedded technical frame** (BTF), which in special cases can be coincident with the BAF. Although embedded in the bone, BTFs may, in fact, have a thoroughly arbitrary and non-repeatable geometric relationship with respect to it. This calls for the acquisition of more information to estimate the spatial location of anatomical landmarks and thus the position and orientation of the BAFs. This information consists of the coordinates of an adequate number of anatomical landmarks in the relevant BTF (*AL parameters*). This procedure is generically called *anatomical landmark calibration* and can be performed when the data acquired come from CT scans as well as from

goniometers or other means such as roentgenographic and anatomical measurements (Andriacchi et al., 1980; Johnston et al., 1979). The experimental protocol based on the above-described approach is referred to with the acronym CAST that stands for "Calibrated Anatomical Systems Technique".

A detailed definition of the Anatomical Landmarks adopted in the frame of the VAKHUM project is given in Annex I.

2.5.1 Description of the procedure

The gait analysis protocol used for the reconstruction of the segment pose and joint kinematics of the lower limb during locomotion is the *Calibrated Anatomical System Technique* (C.A.S.T.) protocol (Cappozzo et al., 1995, Benedetti et al., 1998). The application of the protocol entails the following:

Marker set: Rigid plates, on which are mounted four retroreflective markers, are attached with elastic straps to the trunk, to the pelvis, and to the thigh, shank and foot of both legs.

Data acquisition:

1. At the outset, to record the joint rotation off-set, a standing posture of the subject is collected.
2. Relevant motion tasks are analysed: level walking, stair climbing, rising from a chair, stepping-up, etc.
3. To relate the movement of the marker arrays to the underlying bones, *anatomical calibration* is performed. This entails the location of a number of Anatomical Landmarks (ALs) in the technical frame defined by the plate-mounted markers. The ALs in the pelvis, thigh, shank and foot that are routinely of relevance are listed below (Cappozzo et al., 1995):

Pelvis: left anterior superior iliac spine (LASIS), right anterior superior iliac spine (RASIS), left posterior superior iliac spine (LPSIS), right posterior superior iliac spine (RPSIS), common centre of the femoral head and acetabulum (HJC). **Femur:** prominence of greater trochanter external surface (GT), medial epicondyle (ME), lateral epicondyle (LE), antero-lateral ridge of the patellar surface groove (LP), antero-medial ridge of the patellar surface groove (MP), most distal point of the lateral condyle (LC), most distal point of the medial condyle (MC). **Tibia and fibula:** prominence of the tibial tuberosity (TT), apex of the head of the fibula (HF), most medial ridge of the medial tibial plateau (MMP), most lateral ridge of the lateral tibial plateau (MLP), distal apex of the medial malleolus (MM), distal apex of the lateral malleolus (LM). **Foot :** upper ridge of the calcaneus posterior surface (CA), dorsal aspect of first metatarsal head (FM), dorsal aspect of second metatarsal head (SM), dorsal aspect of fifth metatarsal head (VM).

The locations of the ALs are determined using a pointer on which two markers are mounted at known distance from the tip. The experimenter points the tip of the pointer onto the AL so that the markers on the pointer and the relevant body segment technical markers are visible to the cameras. At least one frame is recorded. This procedure is repeated for each AL.

4. The hip joint centre (HJC) is determined by means of the functional method. The subject is asked to perform continuously and sequentially a flexion-extension followed by an abduction-adduction of both hips at a self-selected speed (Cappozzo 1984, Leardini et al., 1999).

Analysis: Through obvious geometric calculations, and by using the reconstructed position of the pointer markers, the local coordinates of the ALs are determined. The HJC in the pelvic technical frame is estimated as the centre of the optimal spherical surface that fits (in a least square sense) the trajectory of the technical frame origin of the thigh (centroid of the markers). If the functional method is not applicable because of the subject's functional limitations, a prediction approach based on regression equations is used (Bell et al., 1990). The reconstructed trajectories of the ALs allow the anatomical bone embedded frames to be defined as in Cappozzo et al. (1995). Joint angles are then calculated using the Grood and Suntay (1984) convention. The Z-axis of the proximal frame is taken as the flexion-extension axis of the joint rotation, the Y-axis of the distal frame as the internal-external rotation axis, and the axis orthogonal to the previous two at any given instant of time (floating axis) as the abduction-adduction axis. The three axes define the so-called joint coordinate system (JCS).

The procedure easily allows extension/modification of the list of ALs to be tracked.

2.5.2 Methodological qualification

- Accuracy and precision of stereophotogrammetric systems: 1/3000 of the FOV (field of view) diagonal (Ehara, 1995); reconstruction from other markers: 2-4 mm and about 1 mm (MAL test, Della Croce and Cappozzo, 2000).
- Magnitude of the soft tissue artefacts (STA) associated with plate-mounted markers: from 2 to 15 mm (Angeloni et al., 1992).
- Propagation of the STA on the bone orientation: femur [6–20]deg., tibia [4-10]deg. (Cappozzo et al., 1996).
- 3-D precision on AL identification (units in mm): pelvis [3-24], femur [1-19], tibia and fibula [1-20], foot [0.7-21] (Della Croce et al., 1999). Propagation of the AL identification on the orientation of bone anatomical frames: 0.9-9.4 deg (Della Croce et al., 1999).

2.5.3 Data processing flow interfaces

The data will be stored in the database.

Data Description

Specifications, which define a syntax, for Data Storage and Transfer files (DST) have been set for use among the partners participating in the CEC funded CAMARC II research project (Morris, 1994). Consistent with this syntax, a lexicon called Pre-processed Gait Data (PGD) has been defined to allow the storage and exchange of gait data consistent with the proposals made in this report

Data will be exchanged using a lexicon based on the CAMARC DST (*Data Storage and Transfer*) syntax protocol proposed for the storage and the exchange of data files between the laboratories participating in the CEC project CAMARC II (Paul and Morris, 1992). The lexicon was given the acronym **PGD** (*Pre-processed Gait Data*) because, when it was first proposed, it was aimed at reporting gait analysis information (Cappozzo and Della Croce, 1994). The relevant files are based on ASCII code. Although in the present project its use will be extended to other motor acts and may also contain processed data, it was though preferable not to change its original, well-known acronym. Extensions of this lexicon to anatomical landmark trajectories, anatomical frame poses and joint angles will be defined in the course of the project.

The PGD lexicon was aimed at writing files with data concerning the description of the 3-D position and orientation of human bones and/or body segments (head, trunk, pelvis, lower limb bones and upper limb bones), external reaction forces, body-segment inertia parameters, temporal/distance factors, EMG recordings. The original design was purposely created as such to allow further kinematic and dynamic variables to be added.

When designing the lexicon, it was decided that the type of information included in the file should be "device and protocol independent". Thus, each laboratory is free to use its accustomed instrument and experimental protocol of choice. However, the results of the tests must be provided in a standard form, which unavoidably entails pre-processing the measured data. It is important to realise that this pre-processing must not imply a commitment to one description of joint kinematics and dynamics, the choice of which could be changed at any time according to final user preferences.

The format for pre-processed data illustrated in the enclosed Annex is therefore made compatible with most experimental protocols and this allows the use of the same data-processing methodology, that is, the same application software. This means that resulting presentation should be the same irrespective of the specific experimental technique used (marker placement, for instance) and,

therefore, direct comparisons are possible. It should also be noted that this data format embodies the specific experimental protocol used and that this may be unknown to the remote user. In fact, the PGD lexicon makes the kinematic and dynamic variables of each body segment readable without involving any knowledge on the specific set up of the laboratory that has produced them.

As illustrated in Cappozzo et al. (1995), the description of the position and orientation of body segments is based on the concepts of technical frames (constructed using technical marker clusters) and anatomical landmark local coordinates. The latter parameters are determined using anatomical landmark calibration techniques that are typical of each experimental protocol. The anatomical landmarks, the local coordinates of which must be provided, are those defined in Benedetti et al. (1994) and Cappozzo et al. (1995). This document also provides indications on how to identify these landmarks on the subject's body. Technical frame position and orientation and anatomical landmark parameters allow for the calculation of position and orientation of anatomical frames as defined in Cappozzo et al. (1995).

As they are based on ASCII code, DST files require a great deal of memory. Thus, an attempt to make the data as compact as possible was made. For instance, the PGD lexicon reduces the redundancies intrinsic in the marker coordinates and/or in the direction cosines of the orientation matrices of the technical frames by using the position and orientation vectors. Relevant information on how to calculate the orientation vector from the orientation matrix is provided in Spoor et al. (1980).

Some of the parameters/variables to be included in the file may assume only values within given lists. These lists are reported in the Appendix to this document, and, should the need occur, are capable of being updated.

Data Format

For a detailed description of the PGD file see Annex II.

2.6 COLLECTION OF JOINT KINEMATICS DATA

Joint kinematics is collected using custom-made, six-revolute-joint instrumented linkages, or goniometers (Salvia, 2000). Within VAKHUM, most data collection at joint level occurs *in vitro*, though it is anticipated that *in vivo* experiments could also take place.

2.6.1 Description of the procedure

Sections 2.1 *CT data collection* and 2.2 *Data alignment* described the protocol used to perform the collection and alignment of the image datasets ($D_{bone,1}$ and $D_{bone,2 \rightarrow 1}$) for the full leg.

The specimen is then sawn through the central part of the femoral diaphysis. Two parts are obtained: a pelvic part including the hip joint only, and another including knee and ankle joints.

Each joint is a compound of two joint segments (Figure 5):

- Hip joint: *proximal* segment = *pelvis* and *distal* segment = *femoral bone*.
- Knee joint: *proximal* segment = *femoral bone* and *distal* segment = *tibial bone*.
- Ankle joint: *proximal* segment = *tibial bone* and *distal* segment = *talus*.

Each joint is then processed according to the protocol described below.

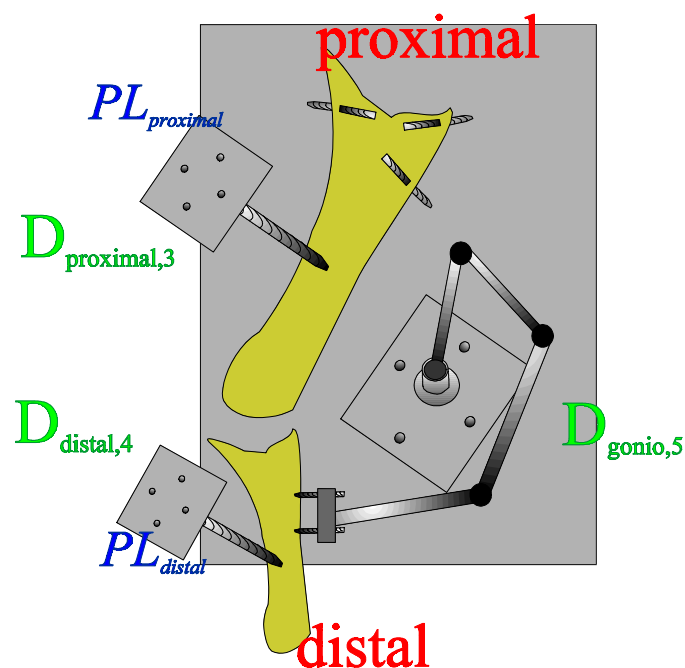


Figure 5. Experimental setup for joint kinematics acquisition and registration. See text for explanations.

Data acquisition:

See Figure 5.

- 1) several image datasets are collected: 1- at the level of the reference plate $Pl_{proximal}$ set in the proximal segment ($D_{proximal,3}$), 2- at the level of the reference plate Pl_{distal} set in the distal segment ($D_{distal,4}$), 3- at the level of the goniometer origin ($D_{gonio,5}$),
- 2) dynamic motions of the joint are performed passively and recorded with the goniometer (sampling rate: 200 Hz).

Analysis:

Registration of the data must take place prior to further activities, to allow anatomical analysis of the results. This is explained in Section 2.7 *Intra CT Registration for Joint Kinematics Data Collection*.

2.6.2 Methodological qualification

The reliability of the goniometers is as follows (Salvia, 2000):

- Static accuracy is better than 0.9° .
- Dynamic accuracy shows a standard deviation of 0.4° with a maximal error of 1.1° .
- Precision of the pivot coordinates is 0.1 mm for the three components and accuracy is better than 1mm.
- Repeatability is 2.8° (SD= 1.0°) for rotation.
- Reproducibility on the pivot X, Y, Z coordinates shows an average standard deviation of 1.2 mm (max SD found: 4.1 mm), 0.9 mm (max SD found: 1.9 mm) and 1.1 mm (max SD found: 2.0 mm) respectively.

2.6.3 Data processing flow interfaces

The data produced in this chapter is used in the kinematics registration procedure within the CT dataset (see Section 2.7 *Intra CT Registration for Collection of Joint Kinematics Data*).

Data description

- Goniometer output is the electrical values of each of the potentiometers during the motion analysis.
- CT scan datasets include:
 - 1- $D_{proximal,3}$: the reference plate $Pl_{proximal}$ inserted into the proximal joint segment,
 - 2- $D_{distal,4}$: the reference plate Pl_{distal} inserted into the distal joint segment
 - 3- $D_{gonio,5}$: the markers located at the goniometer origin to define the local goniometer frame within the current CT frame.

Data format

Raw data produced from the techniques presented in this chapter will not be exchanged. Joint kinematics data will only be exchanged after registration of the data into the CT reference frame (see Section 2.7 *Intra CT Registration for Collection of Joint Kinematics Data*)

2.7 INTRA CT REGISTRATION FOR COLLECTION OF JOINT KINEMATICS DATA

The previous chapters showed that the collection of several CT datasets are necessary:

- 1- the first datasets ($D_{bone,1}$ and $D_{bone,2\rightarrow1}$) include morphological data of the full lower limb with minimal insertion of non natural objects, i.e. pins, (see Section 2.1 *CT Data Collection*) in order to obtain optimal 3D models; alignment of the 3D models are already performed (see Section 2.2 *Data alignment*).
- 2- the fact kinematics analyse requests to stabilize the proximal joint segment as strongly as possible to avoid artefacts, made the use of rigid metallic pins unavoidable; furthermore studying of the hip joint, knee joint and knee joint simultaneously is, for practical reasons, not possible; therefore supplementary CT datasets ($D_{proximal,3}$, $D_{distal,4}$ and $D_{gonio,5}$) are collected as mentioned previously (see Section 2.6 *Collection of Joint Kinematics Data*).

Therefore, the next procedure include several steps: 1- location of the goniometer origin within $D_{bone,1}$; 2- alignment of the goniometer frame along $D_{bone,1}$; 3- definition of the anatomical axis.

2.7.1 Description of the procedure

Location of the goniometer origin

- 1- the spatial coordinates markers $m^{j,gonio}$ $\{j: 0 \rightarrow 3\}$ located at the origin of the goniometer frame are determined from the $D_{gonio,5}$ image dataset (using the *marker location protocol* described in Section 2.2 *Data alignment*),

Alignment of the goniometer frame

- 2- the spatial coordinates of the markers in the proximal reference plate $Pl_{proximal}$ are processed from the $D_{bone,1}$ and $D_{proximal,3}$ image datasets (using the *marker location protocol* described in Section 2.2 *Data alignment*),
- 3- from these locations, an alignment matrix $C_{proximal,3\rightarrow bone,1}$ is found (see Section 2.2 *Data alignment*),

- 4- goniometer data output (see Section 2.6 *Collection of Joint Kinematics Data*) is transformed using $gonio_{bone,1} = C_{proximal,3 \rightarrow bone,1} gonio_{proximal,3}$; joint kinematics data is now located within the same frame ($D_{bone,1}$) as the morphological data.

If necessary, the relative position between of the distal bone segment can be controlled between the different image datasets. The distal segment should remain motionless during and between the acquisition of the image datasets. If it is not the case, the spatial coordinates of the markers in the distal reference plate Pl_{distal} are processed from the $D_{bone,1}$ and $D_{distal,4}$ image datasets (using the marker location protocol described in Section 2.2 *Data alignment*). The alignment of the distal segment can then occur following point 3- and 4- above.

Definition of the anatomical frames

- 5- for each segment, anatomical frames are identified using the same conventions as during the collection of limb kinematics data (see Section 2.5 *Collection of Limb Kinematics Data*); Skeletal Landmarks (SLs) are located directly on the reconstructed 3D models using the mouse cursor within a computer graphics environment; the SLs used within VAKHUM are given in Annex I. A more accurate definition of the landmarks is available in French (Ciavarella, 2000) and will be translated to English later in the project,
- 6- the hip joint centre (HJC) is processed from the $D_{bone,1}$ image dataset; the femoral head is processed as a sphere, the centroid of which is located by image processing (see the *marker location* protocol in Section 2.2 *Data alignment*).

Note that all Skeletal Landmarks should be as similar as possible to the Anatomical Landmarks determined previously (see Section 2.5 *Collection of Limb Kinematics Data*) in order to facilitate WP4.

Analysis: the Skeletal Landmarks are processed in the same way as the Anatomical Landmarks (see Analysis in Section 2.5 *Collection of Limb Kinematics Data*).

2.7.2 Methodological qualification

Location of the goniometer origin

This is similar to the protocol used for *marker location* in Section 2.2 *Data alignment*.

Alignment of the goniometer frame

This is similar to the protocol used to process the *alignment matrix* in Section 2.2 *Data alignment*.

Definition of the anatomical frames

Precision of the identification of the 6 Skeletal Landmarks (SL) on 3D models by several experimenters have been compared with the spatial coordinates of the same SL directly digitised using a industrial Faro arm[®] (Ciavarella, 2000). The averaged deviation was: 1.56 mm (SD = 4.26mm).

Further experiments are currently being performed to quantify the repeatability of the sequences of protocols (*CT Data Collection, Data Alignment, Collection of Joint Kinematics Data, Intra CT Registration for Collection of Joint Kinematics Data*) presented in this report and a report will be produced at a later stage.

2.7.3 Data processing flow interfaces

Data description

Data output will be the displacement of each distal joint segment during a particular motion. The convention used will be the global transformation of the segments and joint angles calculated, as employed by Grood and Suntay (1984).

Data format

Joint kinematics data will be included in a PGD file format, or a modification of it. Further discussion within the consortium should occur to find a consensus.

2.8 MUSCLE MODELLING

Muscle modelling from medical imaging is usually performed with Magnetic Resonance Imaging (MRI), which allows good contrast of the soft tissue. Unfortunately, MRI has two drawbacks: 1- it is limited by the length of the surface coil used around the region of interest; 2- acquisition time is long. Because of these drawbacks, full modelling of long muscles (e.g. biceps femoralis) is practically difficult using MRI. Within VAKHUM, a pilot study will be performed to study the feasibility of another medical-imaging protocol for muscle modelling: CT-scan (Contal, 2000). This allows very fast scanning of wide areas but has some drawbacks: X-ray irradiation and poor definition of the soft tissue. X-ray radiation is not a direct concern within VAKHUM because cadaver specimens are available. The aim of this chapter is to process the CT image dataset in order to increase the image contrast, to digitise muscle contours and to obtain 3D models of the same muscle. Note that this study is not entirely finished at this time and improvements to the method presented below can be expected.

2.8.1 Description of the procedure

Medical imaging: Specimen preparation and CT medical imaging procedure is similar to the protocol described previously (see Section 2.1 *CT Data Collection*).

Image processing: Contrast enhancement is performed by processing the colour look-up-table (LUT) of the full image dataset (Russ, 1995): 1- crop the LUT to select only the intensities related to muscular tissue (typically between 30 and 150 Hounsfield Units); 2- histogram stretching of this cropped LUT.

Segmentation: Structure segmentation is performed fully manually (see Section 2.3.1.3 *Manual protocol*). Sixteen muscles of the pelvis and thigh have been digitised. The average number of digitised points is near 500 for each muscle. Total processing time spent on digitisation alone was about 40 hours. Irregularities of the manual data required further filtration before graphical visualisation or data transformation (e.g. smoothing or deformation of the surfaces). Data filtering was then performed using a surface approximation (see next sub-section) from the contours obtained from the manual segmentation.

Data control: description of the problems and solutions: Initial muscle contour data after manual segmentation is available from ASCII file (see below the *Data format* section). Problems met in the file data can be user related or technical problems.

- User related problems: these relate to a potential lack of logical experience of the operator performing the segmentation:
 1. the Z-value within the same contour is not constant.
 2. the Z-coordinate is not monotonic to the slide number.
 3. self-crossing of the contour data (originally impossible for the muscle tissue).

As this problem is the result of a logical hitch with no repeatable pattern, the best solution is interactive processing of the file exhibiting the problem.

- Technical problems:
 1. the number of points between adjacent contours are different.

Solution: interpolation and recalculation for a preset number of points. The easiest way is to recalculate all the contours with a similar number of points (external parameter from user menu).
 2. the lengths of adjacent contours are different.

Solution: application of a linear approximation of the adjacent contours proportional to the length difference using preset weight coefficients (external parameter from user menu).
 3. orientation of the contours is not homogeneous (clockwise vs. anti-clockwise).

Solution: calculation of the *contour direction index*, by summarizing the cross-product projections of the normal and tangent of the normalized vectors
 4. for each pair of adjacent contours, find the pair of points leading to a minimal distance between the contours.

Solution: search for the closest point of the current contour by weighted criterion including a) the distance between the contours, b) the average length of a fragment and c) the direction of the point normalized vector. For c), it is necessary to locate for each contour a reference point (e.g., the Geometric Centre or GC), which is include within the contour.
 5. the GC is located outside the contour, this may be important for the pseudo-cylindrical coordinate system, especially for the F_i -coordinate if a monotonic behaviour relative to point number is expected.

Solution: search of any point within the contour.

6. similar contours with different Z coordinates; this is more likely to happen for the long muscles when the segmentation result shows pseudo-equivalent cross-sectional areas.

Solution: warning about possible errors.

The problems and solution reported above are not exhaustive, but they reflect the need for a filtration procedure to pre-process the result of manual segmentation prior to mathematical approximation.

The above pre-processing of the input data is partly interactive, partly automated. Automated procedures are implemented: e.g., the smoothing parameters of the coordinate functions can be put independent of both point and contour index. This allows constructing a routine to achieve the preset difference between raw and processed data. Furthermore, a criterion similar to a weighted sum of the difference between the position of the centre of mass, the surface area and the volume is also used. Unfortunately there is not a clear formal criterion for this kind of optimisation. Ultimately, only an expert in Anatomy can assess the quality of the final surface.

Mathematical approximation: From the contours obtained during the segmentation, a mathematical approximation of the surface has been performed. Mathematical background can be found in De Boor, (1978) and Rogers, (1989). Bi-directional (bicubic) splines with preset boundary conditions and sets of weight coefficients are used. This provides the necessary continuity (smoothness) for open-close surfaces and a reliable compromise between interpolation and pure linear regression. Basic bi-directional spline approximation can be used to build a system of coordinates most appropriate to the real data. For example, if muscle contours are available then the coordinate system can be either Cartesian (X, Y, Z) or pseudo-cylindrical (R, F_i, Z) with two independent variables such as the number of the slide from which the contour is digitised and the point or their normalized analogs. The advantage of the Cartesian coordinate system is its natural coincidence with the original CT frame. On the other hand, an asymptotic behaviour of the smoothed data may appear. If the function asymptotically tends to a linear regression plane (usually it is for polynomial spline) then the result is a pure straight line instead of the real muscle volume, and unrealistic deformation of the original data appears. This is not the case if a pseudo-cylindrical coordinate system is used. The latter uses functions including independent asymptotic behaviour for R, F_i and Z . Pseudo-cylindrical convention can also be useful for the purposes of a surface transformation by any physical principle.

2.8.2 Methodological qualification

Medical imaging: See Section 2.1 *CT Data Collection*.

Image processing: No methodological qualification is needed because the image processing procedure did not alter the relative value of the voxels of interest.

Segmentation: The accuracy of the manual segmentation has not been performed. Inter- and intra-operator repeatability of the method has been obtained by asking three independent users to perform the segmentation of the same muscle three times (Contal, 2000). The maximal variation between the operators was 18.0 % which reflects the subjective character of manual segmentation. The maximal intra-operator variability was 6.2 %.

Mathematical approximation: to quantify the deviation of the results after mathematical modelling, sixteen muscle surface were approximated (Contal, 2000). The total volume of each muscle was processed and compared with the volume obtained from the contours directly after manual segmentation. Average deviation was 1.6 % (SD: 0.7, max: 2.7 %, min: 0.5%).

Surface accuracy can also be controlled using other parameters than volume only. The following example shows the output from the mathematical approximation of the sartorius muscle. Ninety three contours were digitised with a range of numbers of points between 10 and 66. Total number of points was 2275. The optimisation parameters during the contour smoothing were 0.000005 and 0.0000006 for (X, Y) and Z directions, respectively. The output below shows the difference between the raw digitised data and the smoothed data.

```
[jambe-dr.couturier--CONTOURS V.2.0], Final
p_{smth}-ang-z = 0.500D-05 0.620D-07
```

***** Digitised data

```
Exp: Fragment length, min, max =>      0.85      6.43  mm
Exp: Fragment average length, min, max =>    1.77      4.23  mm
Exp: Spacing between slices, min, max =>    2.00     12.00  mm
Exp: Contour length, min, max =>      21.71     89.03  mm
Exp: Neighbour cont length dev., min, max => 0.0000     51.12  %
Exp: Contour area, min, max =>      29.77    317.29  mm^2
Exp: Neighbour cont area dev., min, max => 0.0000    152.98  %
```

***** Smoothed data

```
Proc: Fragment length min, max =>      0.07      2.02  mm
Proc: Fragment average length, min, max =>    0.30      1.16  mm
Proc: Spacing between slices, min, max =>    1.52      7.47  mm
Proc: Contour length, min, max =>      22.76     86.81  mm
Proc: Neighbour cont length dev., min, max => 0.0004     26.90  %
Proc: Contour area, min, max =>      32.00    302.27  mm^2
Proc: Neighbour cont area dev., min, max => 0.0099     68.50  %
```

The integral characteristics of the source and processed data can be compared from the following output.

***** Digitised Data

```
Exp: CM x,y,z => ( 15.252 12.828 33.517 ) cm
Exp: CM S,V => 379.946cm^2 112.759cm^3
```

***** Smoothed data

```
Smth: CM x,y,z => ( 15.267 12.839 33.346 ) cm
Smth: CM S,V => 374.500cm^2 112.666cm^3
100.*(abs(Rel Del_{(1-5)}))=>( 0.039 0.027 0.439 1.433 0.083 ) %,
Del_{average} => 0.300 %
```

Overall accuracy: unlike bones, muscles are not rigid: their volume is variable and depends of numerous factors. Therefore, high accuracy on the muscle contours is probably not necessary. On the other hand, muscle direction and attachments are of importance for biomechanical simulation and realistic visualisation (Figure 6).

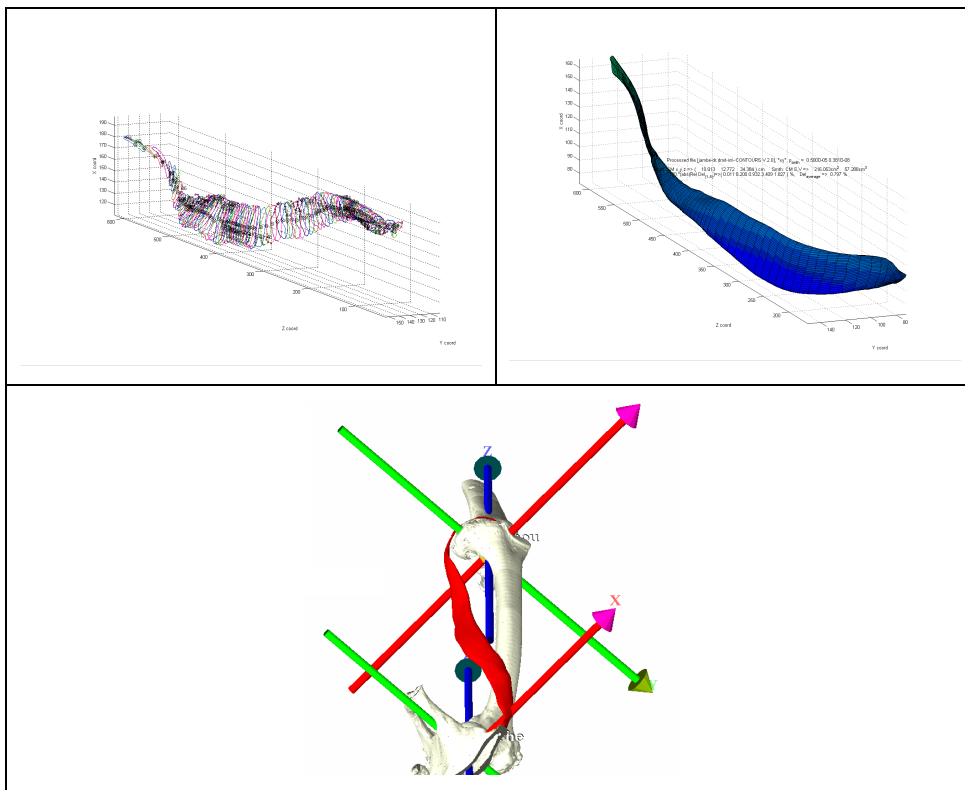


Figure 6. Left: Sartorius muscle. Right: Gracilis muscle. Bottom: Sartorius muscle with isosurface of the pelvis, femoral bone and part of the tibial bone.

2.8.3 Data processing flow interfaces

Data description

Muscle morphological data will be used during the pilot study about muscle modelling. Data includes both raw contours from segmentation and interpolated mathematical surface. It will be available from ASCII files, description of which can be found below.

Data format

- data from manual segmentation

```

CONTOURS V.2.0                                /* file header */
10                                             /* number of points in current contour */
58 0 189.210251 137.820602 36.700001 /* first digitised point of current contour */
58 1 192.788147 137.769547 36.700001 /* 1rst digit = original slice number in CT */
58 2 193.186768 140.397308 36.700001 /* 2d digit = point index in contour */
58 3 192.588486 144.475708 36.700001 /* 3rd digit = X coordinate */
58 4 190.658890 145.221466 36.700001 /* 4th digit = Y coordinate */
58 5 188.035080 145.258911 36.700001 /* 5th digit = Z coordinate */
58 6 186.885254 143.838882 36.700001
58 7 186.689499 142.405258 36.700001
58 8 187.230728 140.242889 36.700001
58 9 188.234741 138.552734 36.700001
12
57 0 181.797562 144.083694 41.700001
57 1 185.577652 144.568680 41.700001
57 2 187.949997 143.354782 41.700001
57 3 190.089005 141.655472 41.700001
57 4 189.403168 138.014755 41.700001
57 5 187.499023 139.956741 41.700001
57 6 185.125107 141.413345 41.700001
57 7 182.762161 141.170914 41.700001
57 8 181.351288 139.957474 41.700001
57 9 179.926331 140.928543 41.700001
57 10 179.209152 142.142227 41.700001
57 11 180.142410 144.083893 41.700001
..... to be continued until the EOF.....
    
```

- data after surface filtering and approximation

```

FACETS V.1.0                                /* file header */
4                                             /* number of vertices in current facet */
189.33945 137.86539 40.03333 /* first interpolated vertex of current facet */
189.05153 137.85445 40.03333 /* 1rst digit = X coordinate */
188.90159 137.89615 36.70000 /* 2d digit = Y coordinate */
189.21025 137.82060 36.70000 /* 3rd digit = Z coordinate */
    
```

4

189.05153 137.85445 40.03333

188.78098 137.98669 40.03333

188.68248 137.97275 36.70000

188.90159 137.89615 36.70000

..... to be continued until the EOF

2.9 FINITE ELEMENT MESH GENERATION

2.9.1 Description of the procedure

For the activities to be performed in the context of the VAKHUM project an advanced implementation of the original hexahedral mesh generator proposed by Tagavi (1996) will be used (Hexar 4.2, Cray Research inc., Minneapolis, USA). This is a grid-based generation algorithm. This class of automatic mesh generators has been deeply discussed in the D3.1 deliverable and will not be repeated here. A description of the specific algorithm adopted follows.

The starting point of the mesh generation process in HEXAR is a triangulated surface definition, called TSD surface. A TSD is a discrete representation of a boundary surface as a collection of triangles that can be easily generated starting from an STL surface. A distinctive feature of the algorithm is that a TSD containing small gaps, overlaps or non-conforming elements can be used without need for clean-up and/or repair. Once the TSD is read, and after topological and geometrical checks are performed, a Cartesian base grid encompassing the surface is created. In the next step, ray tracing inside/outside node tests are conducted to classify outside, inside and intersecting base grid cells. Outside cells are then removed.

In the projection step, boundary nodes of the Cartesian grid are projected on to the TSD, initially using a simple projection. This projection is then improved in order to capture TSD features such as feature edges and vertices that are missing. Feature edges are defined as edges in which the normals of adjacent triangles form an angle greater than a user-defined threshold. Feature nodes are at the end points of feature edges, and feature vertices are feature nodes at which more than two feature edges meet.

During the smoothing stage, grid nodes associated with feature edges are constrained to move along their respective feature edge path. After the projection step, the hexahedral grid that intersected the geometry can become very distorted, degenerated or can even exhibit negative jacobians. This is a well-known problem of grid-based algorithms. A smoothing algorithm is then necessary to improve the mesh.

A laplacian smoothing is applied in HEXAR to boundary nodes, in order to improve the quality of the elements. Boundary nodes are moved and then projected back to the TSD. The resulting mesh is still often not usable for finite element calculation since many rather ill-shaped elements may remain. A further adjustment is needed particularly to improve the quality of the boundary elements. In this second smoothing step the relaxation algorithm does not use the STD information.

Some relaxation algorithms will allow nodes to move freely only on areas of low curvature to minimise the departure from the original geometry, while others will move nodes without respecting the original geometry when attempting to solve difficult situations, for example, unravelling cells with negative Jacobians. Thus, in this step, deviation from the original geometry may occur.

After the finite element model is generated, the CT dataset is used to map the material properties onto the model. A new version of the software Bonemat (Zannoni, 1998) will be used that assign to each element the material properties derived from the bone tissue density at the element location. A density calibration is necessary to relate the density of the bone tissue to the value expressed in Hounsfield Units in the CT dataset. The bone density is then related to the mechanical properties of the bone using a proper experimental relationship. Many relationships can be found in the literature, and the one to be used will be chosen depending on the kind of calibration provided. If calibration is not provided, a reference density derived from literature will be assigned to the highest bone density and the second point for calibration will be the density of water.

2.9.2 Methodological qualification

In the past different tests have been performed to assess the accuracy of the proposed method. In an initial work, (Viceconti, 1998), the HEXAR mesh generator was considered together with three other automatic mesh generators. These were tested on a “Standardised Femur” geometry, which is a solid model in the public domain (Viceconti, 1996). The results were compared with *in vitro* experimental results. To evaluate the accuracy of the method structural displacements and surface stresses predicted by the finite element model were considered. The displacements calculated were compared with the experimental ones and the errors were represented with the displacement percentage error, while surface principal strains at 10 different locations were used to investigate the ability of the FE models to predict the surface stresses. The accuracy of the global surface strain was expressed by the root mean square error (RMSE) of the errors at the 10 control locations. The finest hexa mesh, generated with HEXAR, achieved the best accuracy both in the displacements and in the stress prediction. The accuracy in the displacement was of 1.4%, while the RMSE on the strains was equal to the 9.6% of the maximum measured strain. In this work the automatic mesh generator worked on the geometrical representation of the “Standardised Femur”.

In a follow-up work (Viceconti, 1999) the automatic mesh generator was instead used for the creation of a finite element model of an artificial femur starting from a CT dataset. The artificial femur is made of fibreglass-epoxy composite cortical shell filled with polyurethane foam,

commonly used for biomechanical study *in vitro*. The accuracy of the method was evaluated using an implicit *a posteriori* residual-based error estimate. It was shown that the number of elements with stress residuals larger than the 10% of the peak stress was only 1.8% for the finest mesh. Hence the proposed method has been proved to be able to generate high-quality finite element meshes starting from a tiled surface obtainable from a CT dataset.

All these studies were based on data collected *in vitro*, to allow an evaluation of the accuracy of the model. More recently, the method has been evaluated on data collected *in vivo* (Viceconti, 2000). The study was aimed at assessing the robustness and generality required in real-world applications. At the same time, it was verified that the level of automation and the quality of meshes observed *in vitro* was confirmed for data collected *in vivo*. The proposed method was found very general (it successfully meshed CT data of a phalanx, of an ileum and of a femur) and robust enough to cope with the noisy and incomplete data typical of *in vivo* data collection. Eventual increases of the processing time with respect to the *in vitro* study were overshadowed by the increase of speed due to the adoption of next-generation hardware. Last, but not least, the conditioning of the meshes was not significantly worse than that found using data collected *in vitro*.

The aforementioned BONEMAT program was affected by some limitations, that are relevant when the size of the elements becomes comparable to that of the CT voxels. A new version of the software, which solves this problem, has been recently developed and validated (Taddei, 2000). Changes up to 15% in the predicted stress were observed with the more accurate software.

2.9.3 Data processing flow interfaces

The finite element models will be stored in the database and will be used to perform analyses.

Data description

The finite element models of the different bone segments will be made available for performing finite element analyses. For each segment, five models will be produced at different levels of refinement of the mesh. Each model will be available with material definition based on the original CT dataset.

Data format

The finite element models will be stored in the database in different formats: NEUTRAL file format, NASTRAN input file format and ANSYS input file format. Because of their moderate utility for the project, complete results sets will be archived only at the sites of Partners IOR and

ESI, and not replicated in the VAKHUM database. NASTRAN results file format will be used to exchange results between IOR and ESI. Selected results of relevant simulations will be stored in the database for demonstration purposes or in relation to didactical tutorials. Binary VRML format will be used to report the results as a colour scale mapped over a 3D representation of finite element mesh.

3 REFERENCES

- Andriacchi T.P., Andersson J.B.J., Fermier R.W., Stern D., and Galante J.O., 1980, A study of lower limb mechanics during stair climbing, *J Bone Joint Surg*, 62-A, 749-757.
- Angeloni C., Cappozzo A., Catani F., Leardini A., 1992, Quantification of relative displacement between bones and skin and plate-mounted marker. VIIIth Meeting of European Society of Biomechanics, (Roma 21-24 Giugno 1992), 279.
- Bell, A.L., Petersen, D.R. and Brand, R.A. (1990) A comparison of the accuracy of several hip center location prediction methods, *J. Biomechanics*, 23, 617-621.
- Benedetti M.G., Cappozzo A., Catani F., and Leardini A., 1994, Anatomical Landmark Definition and Identification, CAMARC II Internal Report; March 15.
- Benedetti M.G., Catani F., Leardini A., Pignotti E., Giannini S., 1998, Data management in gait analysis for clinical applications. *Clin. Biomech.*, 13, 204-215.
- Cappozzo, A., 1984, Gait analysis methodology. *Hum. Mov. Sci.*, 3, 25-54.
- Cappozzo A. and Della Croce U., 1994, The PGD Lexicon-version 1.1, CAMARC II Internal Report; May 27.
- Cappozzo A., Catani F., Della Croce U. and Leardini A., 1995, Position and orientation of bones during movement: anatomical frame definition and determination, *Clin. Biomech.*, 10, 171-178.
- Cappozzo A., Catani F., Leardini A., Benedetti M.G., Della Croce U., 1996, Position and orientation of bones during movement: experimental artefacts. *Clin. Biomech.*, 11, 90-100.
- Ciavarella C., 2000, Contribution à l'amélioration de la définition des repères anatomiques du membre inférieur pour leur utilisation dans différents contextes expérimentaux en biomécanique, MSc thesis in Physiotherapy and Rehabilitation, University of Brussels.
- Contal C., 2000, Etude de la faisabilité de la reconstruction tridimensionnelle des tissus musculaires à partir du CT-scan, MSc thesis in Physiotherapy and Rehabilitation, University of Brussels.
- De Boor C., 1978, A Practical Guide to Splines, Springer-Verlag, Berlin and Heidelberg; ISBN: 3540903569.
- Della Croce, U., Cappozzo, A., Kerrigan, D.C., 1999, Pelvis and lower limb anatomical landmark calibration precision and its propagation to bone geometry and joint angles, *Med. & Biol. Eng. & Comput.*, 37, 155-161.

- Della Croce U., Cappozzo A, 2000, A spot-check for estimating stereophotogrammetric errors. *Med. & Biol. Eng. & Comput.*, 38, 260-266.
- Ehara Y., Fujimoto H., Miyazaky S., Tanaka S., Yamamoto S., 1995, Comparison of the performance of 3D camera systems. *Gait & Posture*, 3, 166-169.
- Ellis, R.E., Toksvig-Larsen, S., Marcacci, M., Caramella, D., Fadda, M., 1996, Use of biocompatible fiducial marker in evaluating the accuracy of CT image registration, *Investigative Radiology*, 31, 658-667.
- Grood, E.S. and Suntay, W.J., 1983, A joint coordinate system for the clinical description of three-dimensional motions: Application to the knee, *J. Biomech. Eng., Trans ASME*, 105, 136-144
- Johnston R.C., Brand R.A., and Crowninshield R.D., 1979, Reconstruction of the hip, *J Bone Joint Surg*, 61-A, 639-652.
- Lam, W.C., Yuen, S.Y., 1996, Efficient technique for circle detection using hypothesis filtering and Hough transform, *IEE Processing in Visualization Image Signal Processing*, 143, 292-300.
- Leardini A., Cappozzo A., Catani F., Toksvig-Larsen S., Petitto A, Sforza V., Cassanelli G., Giannini S., 1999, Validation of a functional method for the estimation of the hip joint centre location. *J. of Biomech.*, 32, 99-103
- Lorensen, W.E., Cline, H.E., 1987, Marching cubes: a high resolution 3D surface construction algorithm, *Computer Graphics*, 21, 163-169.
- Morris J. R. W., 1994, Data storage and transmission file syntax and lexicons, CAMARC II Internal Report.
- Paul J.P. and Morris J.R.W., 1992, CAMARC II- Data exchange.What?Why?How?, In: Proceedings of the workshop "CAMARC II: Problems and Perspectives", Rome February 29-March 1,1992, Deliverable N.2.
- Press, W.H., Teukolsky, S.A., Vetterling, W.T., Flannery, B.P., 1992, Numerical Recipes in C, Cambridge University Press, New-York, 59-70.
- Russ, J.C., 1995, The image processing handbook, CRC Press, Boca Raton, 237-247.
- Salvia P., Woestyn L., David J-H, Feipel V., Van Sint Jan S., Klein P., Rooze M., 2000, Analysis of helical axes, pivot and envelope in active wrist circumduction, *Clinical Biomechanics*, 15, 103-111.
- Schroeder W., Martin, K., Lorensen, B., 1998, The visualization toolkit, Prentice Hall, Upper Saddle River, 115-152.

- Söderkvist, I., Per-Ake, W., 1993, Determining the movements of the skeleton using well-configured markers, *Journal of Biomechanics*, 26, 1473-1477.
- Spoor, C.W. and Veldpaus, F.E., 1980, Rigid body motion calculated from spatial co-ordinates of markers, *J. of Biomech.*, 13, 391-393.
- Taddei F. and Viceconti M., 2000., Comparative validation of the BONEMAT procedure, version 2, *IOR Internal Report*.
- Tagavi R., 1996, Automatic, parallel and fault tolerant mesh generation from CAD, *Engineering with Computers*, 12, 178-185.
- Viceconti M., Casali M., Massari B., Cristofolini L., Bassini S., Toni A., 1996, The “Standardised Femur program” proposal for a reference geometry to be used for the creation of finite element models of the femur, *J Biomech.*, 29 (9),1241.
- Viceconti M., Bellingeri L., Cristofolini L., Toni A., 1998, A comparative study on different methods of automatic mesh generation of human femurs, *Medical Engineering and Physics*, 20, 1-10.
- Viceconti M., Zannoni C., Testi D. and Cappello A., 1999, A new method for the automatic mesh generation of bone segments from CT data, *J. Med. Eng. Technol.*, 23(2), 77-81.
- Viceconti M., Davinelli M, Taddei F. and Cappello A., 2000., Validation of a method for the automatic generation of patient-specific finite element models from CT data, *IOR Internal Report*.
- Zannoni C., Mantovani R., Viceconti M., 1998, Material properties assignment to finite element models of bone structures: a new method, *Medical Engineering and Physics*, 20(10), 735-40.